AU: Met., Env. & Arid Land Agric. Sci., Vol. **34** No. 1, pp: 203 - 221 (2025 A.D.)
DOI: 10.4197/Met. 34-1.11

Assessing WRF Model Performance for a Severe Case of Rainfall in Western Saudi Arabia

Ahmad E. Samman[1,2], Abdallah Abdaldym[2], and Mostafa Morsy[2]
[1]*Department of Meteorology, Faculty of Environmental Sciences, King Abdulaziz University, Jeddah, 21589. Saudi Arabia.*
[2]*Center of Excellence for Climate Change Research, King Abdulaziz University, Jeddah 21589, Saudi Arabia*

Abstract. this article examines the effectiveness of the Weather Research and Forecasting (WRF) model in simulating a severe weather event across western Saudi Arabia on May 8, 2014, marked by heavy rainfall and thunderstorms. During this event, Makkah meteorological station recorded approximately 50 mm of rainfall accompanied by thunderstorms, posing significant forecasting challenges. The model was configured with moderate to high-resolution settings and various parameterizations in order to replicate the event, and its results were compared with observed meteorological data. Key model outputs, including precipitation intensity and distribution, were analyzed to assess the model's accuracy and its capability to capture critical atmospheric dynamics associated with heavy rainfall in arid regions. The simulated rainfall produced by the experiment demonstrates strong alignment with the Tropical Rainfall Measurement Mission (TRMM) rainfall estimates, both in terms of intensity and the spatial and temporal distribution patterns. This agreement indicates the model's capability to reasonably capture the key characteristics of the rainfall event under study. The findings highlight the strengths and limitations of the model for severe weather prediction in western Saudi Arabia, providing insights into optimal configurations for forecasting similar events in the future.

Keywords: WRF; heavy rainfall; Red Sea trough; Saudi Arabia; cyclogenesis

Introduction

The eastern Mediterranean (EM) area, characterized by its surrounding arid landscapes, mountains, and orographic barriers, is globally recognized as a significant cyclogenetic zone due to its atmospheric conditions that favor the development of low-pressure systems (Ribó and Llasat, 2009). Precipitation in Saudi Arabia (SA) is mostly caused by synoptic-scale disturbances connected to the Red Sea Trough's (RST) (the northward extension of the Sudan monsoon low) incursion into the EM, and it occurs largely between November and April. These disturbances are linked to warm, humid southerly winds that come from tropical areas (El-Fandy, 1948). The trough at upper-level in mid-latitude and the RST are well-established systems linked to cyclogenesis in the EM region. (Abdeldym et al., 2019). The genesis and evolution of cyclogenetic systems, along with associated rainfall events, over SA, particularly in the western regions, are primarily governed by the distinctive environmental and atmospheric conditions influenced by the characteristics and topography of the Red Sea (RS) region (Haggag and El-Badry, 2009; Hasanean and Almazroui, 2015; Almazroui et al., 2018, Samman and Gallus, 2017). The development of these convective

systems is influenced by a complex interplay of dynamic and environmental factors. Key contributors include the formation of cyclonic systems over the Mediterranean, which drive atmospheric instability, and the presence of anticyclonic systems over the Arabian Peninsula (AP), which modulate regional airflows and moisture transport, collectively shaping the intensity and spatial distribution of convection (El Kenawy et al., 2014; De Vries et al., 2013). Additional factors contributing to the development of convective activity include an abundance of moisture in the upper troposphere, anomalously elevated sea surface temperatures in the RS, and the modifying effects of local topography. Together, these elements enhance atmospheric instability, intensify vertical motion, and create the favorable environmental conditions necessary for robust convective development and precipitation. (Deng et al., 2015; Al-Mutairi et al. 2019). The convergence of warm and humid air over the RS creates an environment highly conducive to intense convection. The accumulation of humid air supports the development of powerful updrafts, significantly amplifying storm intensity. This effect is particularly pronounced in western SA, where the combination of atmospheric instability and abundant moisture provides ideal conditions for severe weather events (Almazroui, 2011; Al-Mutairi et al. 2019). According to Abdeldym et al. (2019), the rotational part of moisture flux has two primary origins: the Indian Ocean, encompassing the Gulf of Aden and Arabian Sea, and the region encompassing the Mediterranean Sea and Atlantic Ocean.

The characteristics and variability of rainfall across different regions of SA have been extensively studied, including the work of Al-Khalaf and Abdel Basset (2013) and related references. These studies have utilized various numerical weather prediction models (NWP) to examine the meso-scale systems and cyclogenesis processes associated with rainfall patterns (Haggag and El-Badry, 2009; De Vries et al., 2013; Almazroui, 2011). Regional climate models (RCMs) have emerged as a critical method for refining simulations of global climate and reanalysis data, enabling the generation of high-resolution regional climate information. By nesting these models within the broader framework of global datasets, RCMs capture localized climate dynamics, such as topographic influences, land-sea interactions, and small-scale atmospheric processes, which are often not resolved in global models. This approach provides a more detailed and accurate representation of regional climate conditions, making RCMs essential for studying localized weather patterns and assessing climate change impacts at finer spatial scales. The accuracy and reliability of RCMs simulations are heavily influenced by several key factors, including the computational domain size, the placement and configuration of lateral and initial boundaries, the temporal and spatial resolution of the model, and the quality of the forcing fields used as inputs. The domain size determines the extent of the region being analyzed, while the positioning of lateral boundaries impacts the interaction between the regional model and external global data. Utilizing higher spatial resolution enables the model to more accurately capture small-scale processes, including the intricate effects of land use and topographical variations, which play a crucial role in shaping localized weather patterns. Simultaneously, the quality of forcing fields, such as initial and boundary conditions derived from global datasets, is critical in driving the model's performance. High-quality forcing data ensures that the model outputs closely align with observed climatic and meteorological phenomena, thereby enhancing the reliability and accuracy of the simulations (Giorgi et al., 1994; Leung et al., 1999; Sylla et al., 2009). Jones et al. (1995) emphasized that the computational domain should be adequately expansive to facilitate the complete development of features at the fine scale in the region of interest. Seth and Giorgi (1998) emphasized that the appropriate placement of lateral boundaries, at a sufficient distance from the interest zone, is crucial

to escape unrealistic responses arising from interior forcing within the model domain. Conversely, a smaller domain can limit the model's ability to represent internal, higher resolution forcing, potentially leading to unrealistic results (Giorgi and Mearns, 1999). Additionally, Nobre et al. (2001) observed that the accuracy of their simulations was significantly influenced by both the spatial resolution of the RCMs and the placement of the lateral boundaries. Additionally, the findings of Shiao and Juang (2006) demonstrated that the size of the simulation domain exerts a more significant influence on the modeled large-scale atmospheric circulation and the spatial distribution of rainfall compared to the impact of horizontal resolution. This underscores the importance of selecting an appropriately large domain to ensure that the model adequately captures the interactions between regional and larger-scale meteorological processes, which are critical for accurately simulating precipitation patterns. Sylla et al. (2010) proposed that the improved performance of their simulation with a relatively large domain could be attributed to the use of higher-quality reanalysis data at the model boundaries. The discussion highlights the critical importance of domain size, lateral boundary location, resolution, and forcing data quality in influencing the functioning of RCMs. Furthermore, Almazroui et al. (2018) conducted an in-depth investigation into the role of topography and surface heat exchange in the evolution of a significant heavy rainfall event that occurred over Jeddah, SA, on November 25, 2009. Utilizing the Weather Research and Forecasting (WRF) model, their study analyzed how these physical factors influenced the meteorological dynamics and processes contributing to the event's intensity and spatial distribution of precipitation. They showed that the topography of the RS and surface heat exchange played a significant role in shaping both the intensity and spatial distribution of the rainfall over Jeddah. In addition, Deng et al. (2015) studied two other severe rainfall events over SA, which occurred on December 30, 2010, and January 14, 2011, using WRF model. Their findings demonstrated that the model adequately captured the convective mechanisms causing the storms and successfully recreated the three periods of intense rainfall. Al-Mutairi et al. (2019) performed a comprehensive sensitivity study to examine the impact of the RS topography and water body on the development and precipitation associated with a cyclogenesis event that occurred over SA from November 16 to 18, 2015. Their analysis demonstrated a strong alignment between the simulated rainfall and estimates from the Tropical Rainfall Measuring Mission (TRMM) data, accurately capturing both the intensity and spatial distribution of rainfall. Notably, the absence of topography in the model simulations led to unexpected changes in the spatial distribution and intensity of extreme rainfall events, particularly over central and northern SA.

This article primarily aims to examine the performance of WRF model in replicating a significant rainfall event that impacted western SA on May 8, 2014. During this event, the Makkah meteorological station observed intense thunderstorms and recorded close to 50 mm of rainfall. By evaluating how well the model simulates these atmospheric conditions, the study seeks to understand its effectiveness in predicting severe weather events in the region.

1. Data and Methodology

1.1. Data Used

The present study utilized three primary datasets. The first dataset comprised the ERA5 reanalysis data ECMWF (Hersbach et al., 2020). This dataset provided six-hourly observations of horizontal (u, v) and vertical (w) wind components, temperature, and geopotential height at ten pressure levels,

ranging from 1000 hPa to 100 hPa, with a horizontal resolution of 1° × 1°. The spatial coverage encompassed the region extending from 20°W to 70°E and 5° to 70°N from 6th to 12th May 2014. This dataset served as a crucial resource for conducting synoptic analysis and evaluating the model's capacity to accurately reproduce the system of cyclogenesis. Daily precipitation data derived from the TRMM 3B42-Version 7 product (Huffman et al., 2010), characterized by a 0.25° x 0.25° horizontal resolution, were employed to evaluate the simulated rainfall generated by WRF model during the occurrence of the selected severe precipitation event.

WRF model utilized high-resolution static input data, including land use information, soil parameters, and orography, derived from the United States Geological Survey (USGS) database with a resolution of 2 arcminutes. Both the initial and subsequent boundary conditions for the model were obtained from the NCEP Global Reanalysis dataset, which provides data with a 1° × 1° (spatial) and 6 hours (temporal) resolution. The simulation of WRF encompassed a comprehensive suite of meteorological parameters. These included three-dimensional meteorological at 27 distinct pressure levels. Furthermore, the model utilized four layers of soil data, enabling detailed representation of soil moisture and thermal properties. Additionally, the simulation incorporated meteorological variables at the surface providing essential information about surface conditions and atmospheric interactions. To ensure consistency across the simulation, fixed sea surface temperatures derived from the NCEP dataset were used through the entire modeling process. This approach, as outlined by Chawla et al. (2018), allowed for the standardization of oceanic conditions, ensuring that variations in sea surface temperature did not influence the results and maintaining a controlled environment for the study.

1.2. WRF Overview, Configuration, and Setup

WRF model is a popular mesoscale NWP system that is used by the scientific community as well as operational meteorologists (Mohan and Sati, 2016). Developed through a collaborative effort among several leading institutions in the United States, including NCAR, NCEP, and the FSL, the WRF has become a crucial tool for weather forecasting and atmospheric research. The Advanced Research WRF (ARW) core and the Nonhydrostatic Mesoscale Model (NMM) core are the two main dynamical cores that are incorporated into the WRF model. The ARW core employed in this study operates on a fully compressible, Eulerian framework designed to solve the non-hydrostatic equations of motion, ensuring accurate representation of atmospheric dynamics. It uses a terrain-following vertical coordinate system, based on hydrostatic pressure, which enables the model to effectively simulate a wide range of atmospheric phenomena. This configuration allows the model to accurately capture short-lived and extreme events, such as heavy precipitation, severe thunderstorms, and cyclones, making it highly suitable for mesoscale weather simulations and studies of localized atmospheric processes.

The synoptic patterns, mesoscale weather systems, and rainfall distribution over the study area (Figure 1) were simulated using WRF-ARW version 4.6.0 for the period of May 6–12, 2014. This broad domain was strategically chosen to provide a comprehensive understanding of the synoptic conditions and mesoscale weather systems that contributed to the rainfall event over SA. To achieve a higher level of spatial detail, an internal domain with increased resolution was incorporated. The outside domain had a resolution of approximately 36 km, while the nested internal domain featured

a finer resolution of about 12 km, allowing for more precise simulation of localized weather features and the dynamics associated with the rainfall event. The model was configured with a 120-second time step and integrated for 168 hours, starting from 00Z on May 6, 2014. As a spin-up time, the first twenty-four hours were eliminated (Maussion et al., 2014).

The model was configured with several advanced physical parameterizations to accurately simulate the extreme rainfall event. For microphysics, the Ferrier (new Eta) scheme (Aligo et al., 2018) was used, which accounts for cloud microphysical processes, including the formation of precipitation. The radiation scheme employed was the Rapid Radiative Transfer Model for GCMs (RRTMG) (Iacono et al., 2008), which accurately simulates both shortwave and longwave radiation processes in the atmosphere. For the surface, the Monin-Obukhov scheme (Monin and Obukhov, 1954) was applied, providing a detailed representation of turbulence and heat flux exchanges between the atmosphere and the surface. The WRF also incorporated the five-layer thermal diffusion land surface model (Dudhia, 1996) to simulate the interactions between the land surface and the atmosphere, including processes such as soil temperature and moisture dynamics. The PBL (Planetary Boundary Layer) scheme chosen for this study was the Yonsei University (YSU) PBL scheme (Hong et al., 2006), which is effective at modeling vertical mixing and boundary layer dynamics. Additionally, the Kain-Fritsch cumulus parameterization scheme (Kain, 2004) was implemented to represent deep convection and the associated cloud and precipitation processes, crucial for capturing the intensity and distribution of rainfall during the extreme event. These combined schemes allowed the WRF to capture the complex interactions and dynamics involved in the extreme rainfall event accurately.

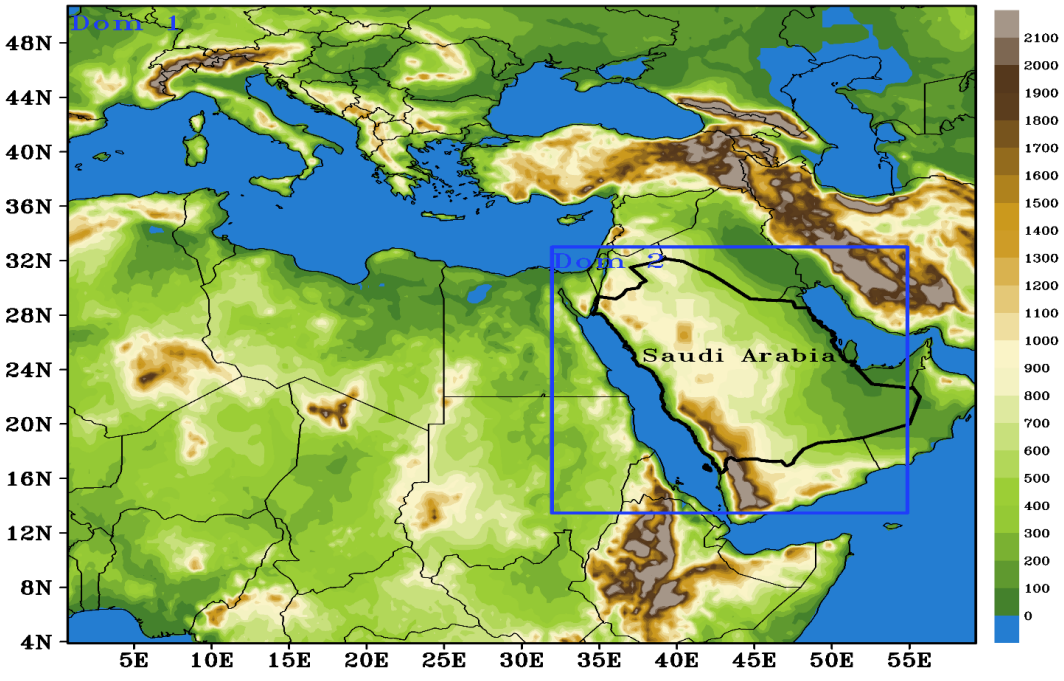

Figure 1 Geographical map of the study area (first domain). Shaded areas represent surface topography (in meters), while the blue box outlines the second domain used for WRF model simulations.

2. Results and Discussion

2.1. Synoptic Discussion

The cyclogenesis event analyzed in this study depicts a typical situation observed over the EM where the interaction between an upper-level mid-latitude cyclone and RST plays a crucial role. Figures 2 and 3 present the temperature (°C) and geopotential height (gpm) at 1000 hPa and 500 hPa, respectively. Figure 4 shows the horizontal distribution of temperature advection and geopotential height (gpm) at 850 hPa. Furthermore, Figure 4 highlights the region of baroclinicity in the lower levels during the study period. At 00Z on May 7, 2014, the subtropical high dominated much of North Africa and the Mediterranean region, exerting its influence over a wide area with stable atmospheric conditions (Figure 2a). Simultaneously, the Siberian high was centered over Turkey and the Black Sea, contributing to cooler, stable air masses in this area. Conversely, the extension of Sudan monsoon low (RST) extended into southeastern Egypt and the RS region. This low-pressure system created favorable conditions for the convergence of moist air, setting the stage for potential convective activity in the affected areas. The northward oscillation of the RST is clearly depicted by the movement of the 100 gpm contour line (represented by the green line) in Figure 2. This oscillation highlights the expansion of the low-pressure system toward higher latitudes. Furthermore, a pronounced thermal gradient, indicated by the red contour lines, is evident in association with the RST. This gradient extends zonally across northern Sudan and southern SA, emphasizing the stark temperature contrasts in these regions and the dynamic atmospheric processes linked to the trough (Figure 2a). At 00Z on May 7, 2014, a mid-latitude cyclone and its associated trough were prominently observed at the 500 hPa level over the eastern region of Europe (Figure 3a). The trough associated with this cyclone exhibited a pronounced tilt, extending from northeastern Turkey southwestward, stretching across northern Libya and Egypt. This configuration highlights the cyclonic influence over a broad area, with the trough's southwestward extension suggesting the potential for dynamic atmospheric interactions and energy transfer across these regions. A distinct temperature gradient extends across western and central SA, linked to the northward oscillation of the RST (Figure 4a). This thermal gradient indicates significant temperature contrasts in these areas, driven by the dynamic interaction between the warm, moist air from the south and the cooler, drier air from the north. The gradient's presence across such a wide area underscores its critical role in shaping the atmospheric conditions conducive to convective activity and potential precipitation events. During the next 12 hours (12Z07 May), a significant temperature gradient will develop across most of SA and eastern part of Sudan (Figure 4b). At the same time, at the 1000 hPa level, the subtropical high weakens, the Siberian high moves eastward, and the RST steadily progresses northward (Figure 2b). Figure 4b illustrates the presence of a region of cold air advection over North Africa, indicating the southward transport of cooler air masses, while warm air advection dominated most of the AP, signifying the northward movement of warmer air. Meanwhile, the cut-off low at 500 hPa began to intensify and shift eastward, extending its influence over northern Libya and Egypt (northwestern part) (Figure 3b). This progress was closely linked to cold air advection originating from northern Europe, which contributed to the development of the upper-level trough. The simultaneous intensification of surface (1000 hPa) and upper-level pressure systems commenced at 12Z on May 7, 2014, and persisted until May 10, 2014, marking a period of significant atmospheric dynamism and interaction between the synoptic-scale systems.

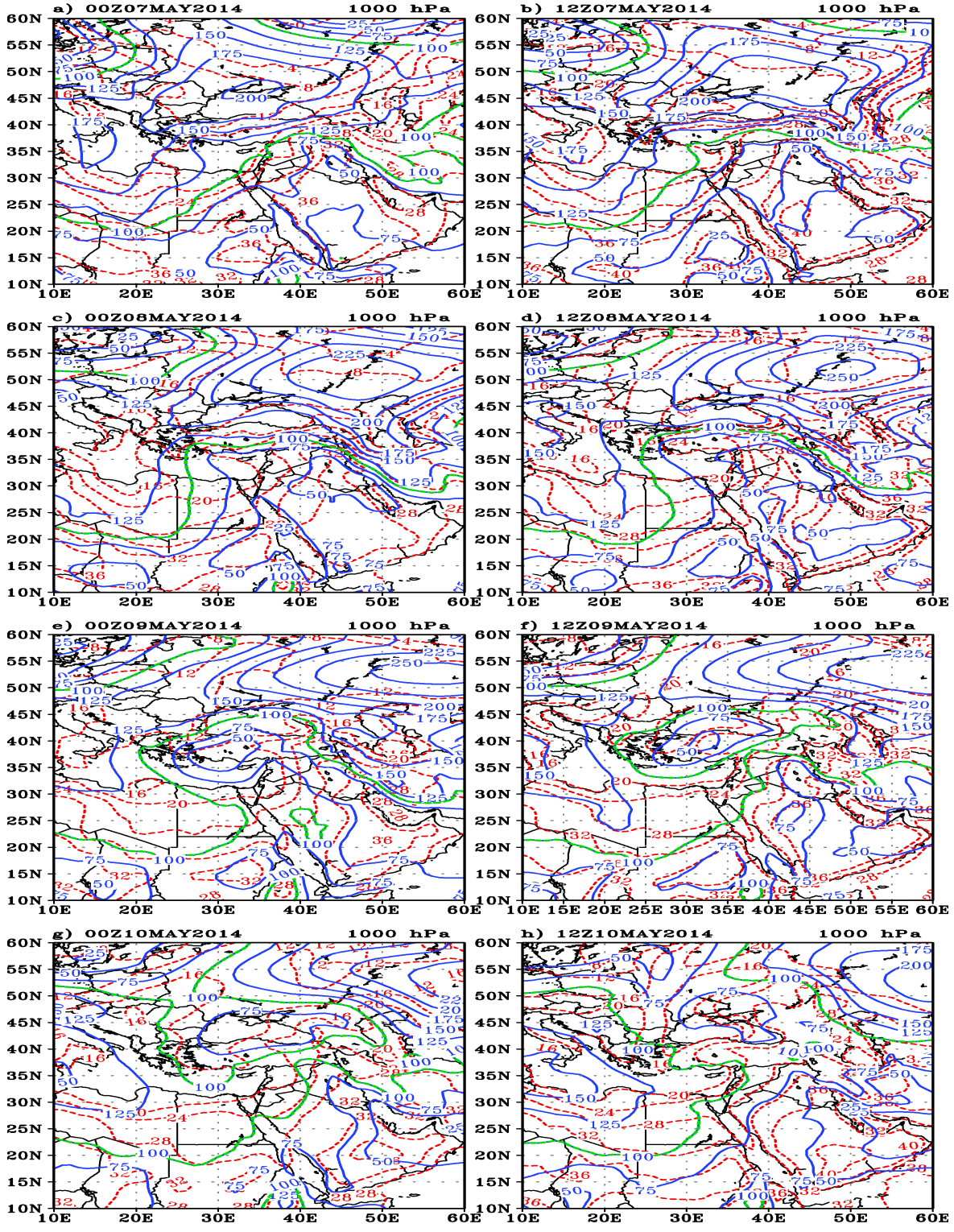

Figure 2. 1000 hPa height contours (solid blue lines) and temperature (red dotted) at 00Z and 12Z for 07 to 10 May 2014.

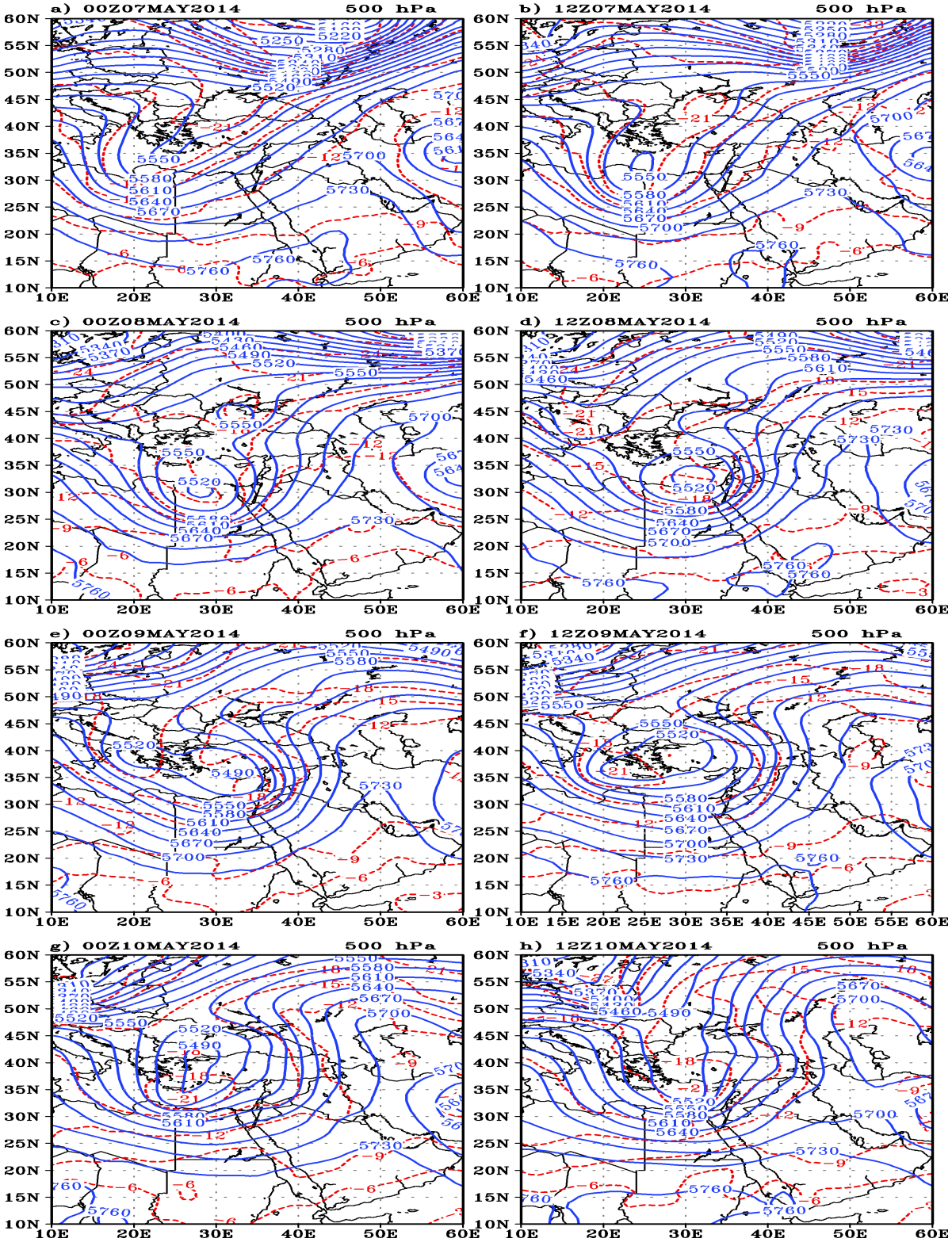

Figure 3. 500 hPa geopotential height contours (solid blue lines) and temperature (red dotted) at 00Z and 12Z for 07 to 10 May 2014.

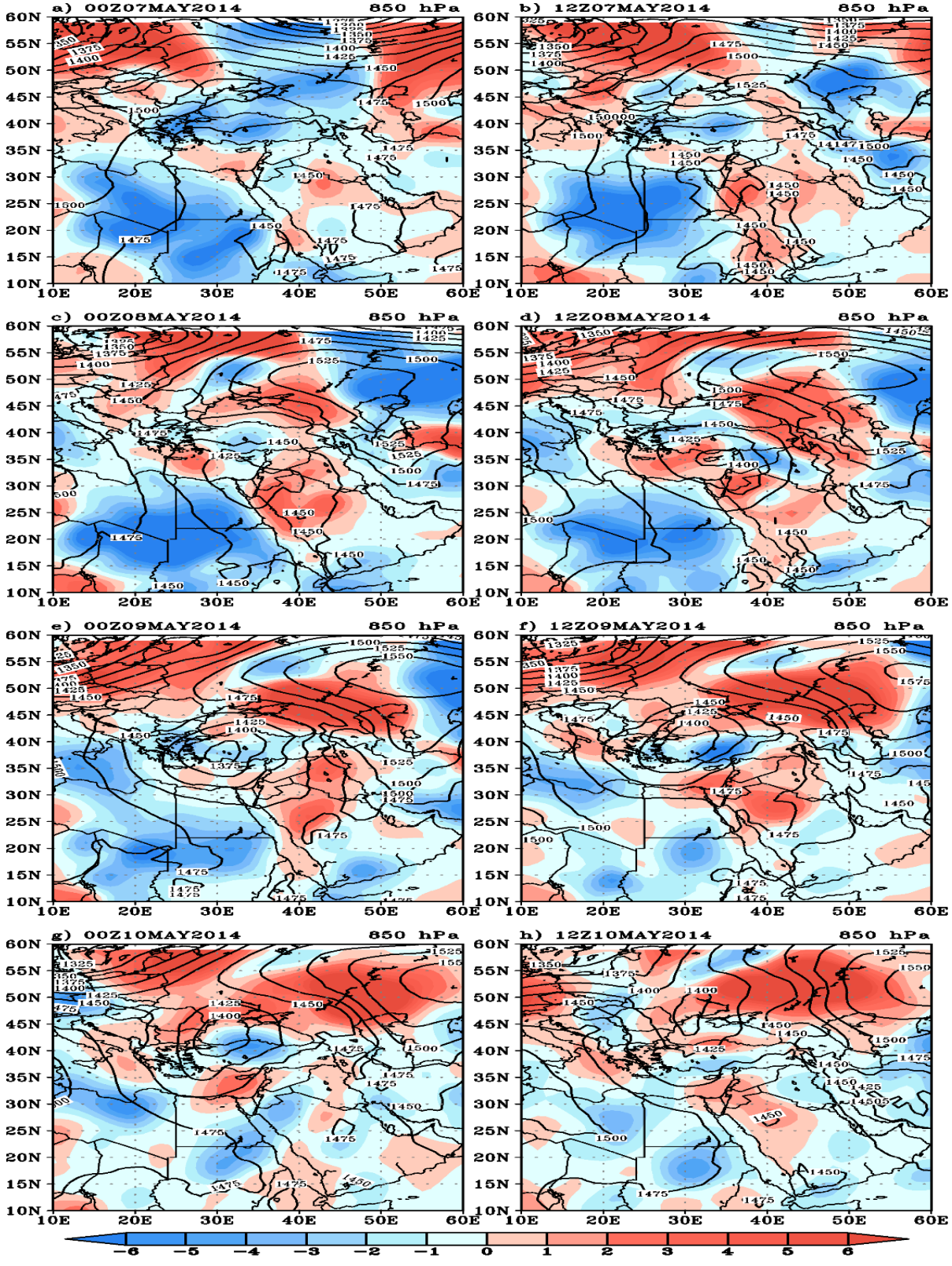

Figure 4. 850 hPa height contours (solid) and temperature advection (shaded) at 00Z and 12Z for 07 to 10 May 2014

At 00Z on May 8, 2014, the surface RST extended northward, significantly influencing the northern regions of the study area, which included Egypt, the EM, and SA. The Sudan Low, positioned centrally over the Red Sea, was characterized by a geopotential height of 25 gpm at its core (Figure 2c), highlighting its prominence in the region's atmospheric dynamics. Concurrently, the cut-off low at 500 hPa continued to intensify, deepening further as it advanced slowly eastward. By this time, it encompassed northern Egypt, with its center marked by a geopotential height of 5520 gpm (Figure 3c). This configuration highlights the enhanced interaction between surface and upper-level systems, contributing to the evolving synoptic conditions in the region. At the 850 hPa level, the advection regions (cold and warm) exhibited a slight eastward shift in response to the shifting atmospheric system. A notable area of intense cold advection developed over Egypt and SA, extending into the Red Sea region. Meanwhile, the warm advection region shifted southeastward, reflecting the dynamic redistribution of air masses as the system progressed across the area. This movement of cold and warm air is indicative of the evolving pressure patterns and the intensifying atmospheric interaction within the region. At the 1000 hPa level, the extension of the pressure system to the north became more pronounced, with the 100-gpm contour line reaching the northern Mediterranean, displaying a broader zonal distribution. This expansion facilitated the formation of a cut-off low over eastern Egypt and the northern Red Sea, where the atmospheric dynamics converged to create a distinct low-pressure system. The northward and zonal extension of the pressure contours contributed to the intensification of this cut-off low, highlighting the significant changes in the atmospheric structure at this level. During the period from 12Z on May 8, 2014, to 12Z on May 9, 2014 (when it rains), a robust interaction occurred between the stretched RST, which originated in the tropical region (Figures 2d, e, f, and g), and the upper-air trough (Figures 3d–g). This interaction became increasingly powerful as the two systems—the RST and the upper-air trough—merged into a single, more powerful system. The primary role of the extended RST was to transport warm, moist tropical air northward, while the upper-air trough contributed a robust cold advection from the polar region, pushing cold air southward (Figures 4d–f). The convergence of these polar cold air and tropical warm air significantly intensified atmospheric instability over the EM and SA. Heavy rains developed as a result of this interaction, with the peak precipitation occurring between 12Z on May 8 and 12Z on May 9 (Figure 5). After 12Z on May 10, 2014, the upper-air trough moved northeastward, and the RST shifted southwestward (Figures 2h and 3h). As a result, the interaction between the two systems dissipated, and atmospheric stability returned, with the high-pressure dominating the region once again.

2.2. Comparison of Rain from WRF and Satellite data

Figure 5 shows the horizontal distribution of accumulated daily rainfall from the TRMM in the left column and the WRF in the right column. TRMM provides observed rainfall data based on satellite measurements, so it is also capable of identifying where rainfall is occurring, especially in areas with limited or nonexistent ground-based observations. However, TRMM's measurements are subject to certain limitations, such as the inability to capture rainfall in areas with thick cloud cover or areas with very low rainfall. Nonetheless, TRMM provides valuable data on the global

distribution of rainfall, and its high resolution allows it to capture local variability to some extent, though it may still miss some fine-scale features that ground-based or high-resolution models like WRF can resolve.

On 07 May 2014, no rainfall was recorded at Makkah and Madinah stations. TRMM data (Figure 5a) indicated significant rainfall in two primary regions within the study area: East Africa and the EM region, which includes Sinai, the Levant, and northern SA. The maximum rainfall intensity reached approximately 40 mm.

On May 7, 2014, no rainfall was observed at the Makkah and Madinah meteorological stations. However, TRMM satellite data (Figure 5a) indicated notable rainfall in two main regions within the study domain: East Africa and the EM region, encompassing Sinai, the Levant, and northern SA. The highest recorded rainfall intensity reached approximately 40 mm. The model output successfully reproduced the intensity and horizontal distribution of the rainfall but displayed a slight eastward displacement (Figure 5b). Additionally, the model output revealed a broader rainfall coverage compared to the satellite data, particularly over Egypt and western SA. This suggests that the model overestimated the extent of the rainfall, making it appear more widespread than what was observed in the TRMM data. On May 8, 2014, Makkah recorded a significant rainfall total of 50 mm, while Madinah registered 4 mm. TRMM satellite data indicated approximately 30 mm of rainfall over Makkah and similar amounts over Madinah (Figure 5c). The TRMM data also identified rainfall over the mid-western and northeastern regions of SA, with intensities ranging from 0 to 30 mm. The model output effectively captured the rainfall distribution in the EM region, although it exhibited a slight underestimation in intensity and a southeastward displacement (Figure 5d). In contrast, the model showed higher rainfall quantities over the central area of SA, with the rainfall pattern shifting toward the north compared to the satellite observations. This suggests some discrepancies in the model's simulation, particularly in central and northern areas. On May 9, 2014, no rainfall was recorded at the Makkah or Madinah meteorological stations. However, TRMM satellite data indicated light rainfall in SA (central part) (Figure 5e). The WRF output also detected rainfall in this area, though it simulated slightly higher intensities compared to the observations from the TRMM data (Figure 5e). This discrepancy highlights the model's tendency to overestimate rainfall intensity in certain areas, despite generally capturing the spatial distribution of precipitation events. Overall, the WRF simulation demonstrates a reasonable capability to predict the horizontal distribution of rainfall, demonstrating a comparatively high degree of agreement with TRMM data. Nevertheless, the model's daily rainfall forecasts typically overshot by 10% to 20% the equivalent total daily values that TRMM records. This overestimation is particularly pronounced in areas experiencing maximum rainfall, such as the RS region and the northwestern parts of SA. This suggests that while the model effectively captures general rainfall patterns, it exhibits a tendency to amplify rainfall intensities in regions of peak precipitation. This overestimation is a common challenge in NWP models, especially when simulating localized convective systems influenced by complex topography. Several factors may contribute to this overestimation. One factor is the convective parameterization; WRF's convective schemes may struggle to accurately represent intense convective processes, leading to the overestimation of heavy rainfall events. Another factor is spatial resolution: coarser model resolutions limit the ability to capture localized rainfall, especially in mountainous regions or areas with complex terrain. Furthermore, model parameterization plays an important role; the physical parameterizations used in WRF, such as cloud microphysics and radiation schemes, may not be optimally tuned for the specific conditions of the Red Sea area and northwest SA. Additionally, the model settings

including the boundary and initial conditions used in the model can significantly affect its performance. Inaccurate or incomplete initial and boundary data can lead to errors in rainfall predictions. Addressing these factors through improvements in model physics, higher resolution simulations, and more accurate boundary and initial conditions can potentially enhance the accuracy of WRF rainfall predictions in these regions.

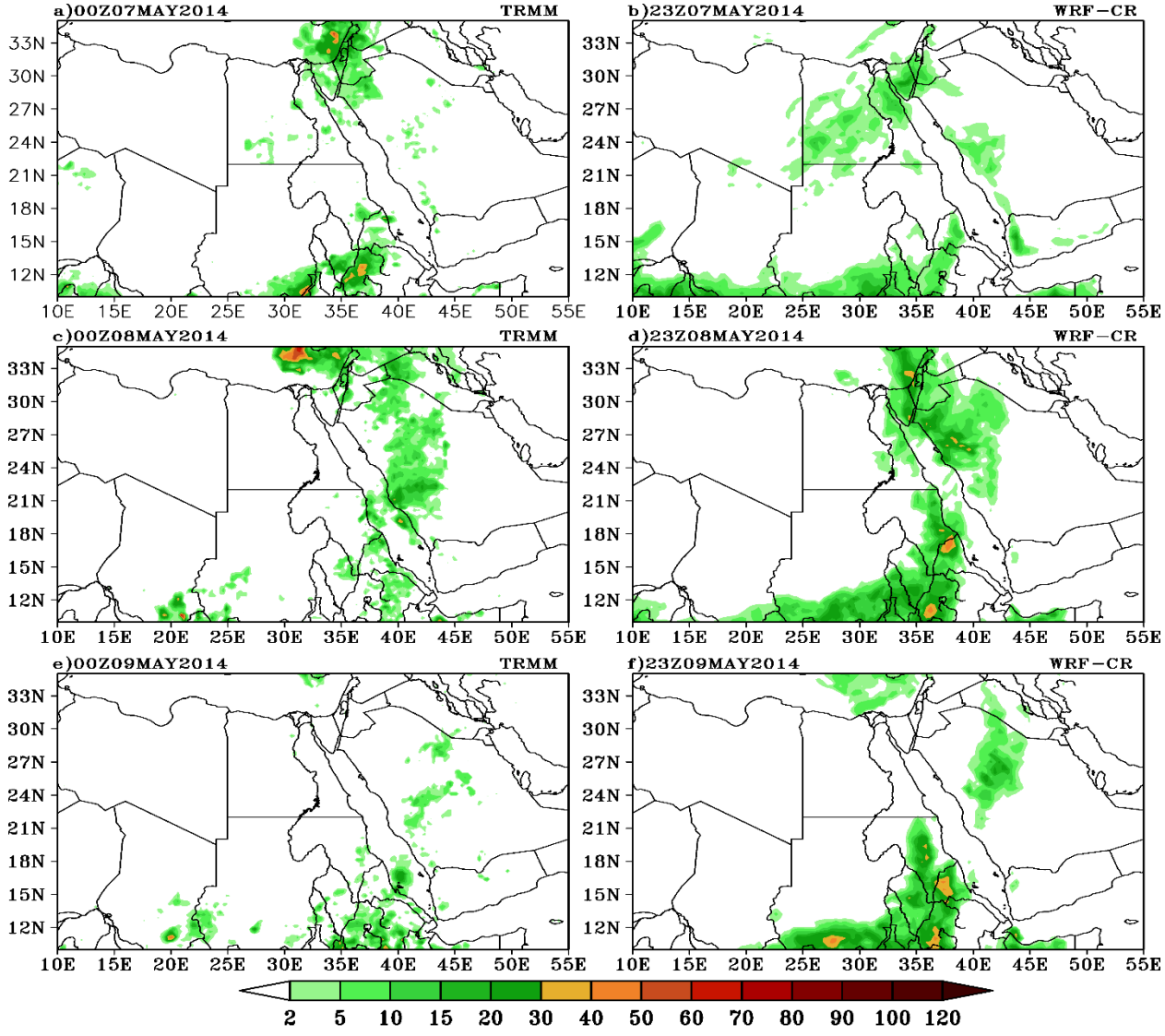

Figure 5. The accumulated daily rainfall from the TRMM dataset and the WRF output for the period 07–09 May 2014.

2.3. Comparison of Synoptic fature from WRF and ERA5 data

To further evaluate and validate the accuracy of the WRF simulation, a comparative analysis was conducted between the synoptic patterns of geopotential height and temperature gradient by the WRF and those derived from the ERA5 reanalysis dataset. Specifically, the temperature gradient and geopotential height fields at 1000 hPa (Figure 6), 500 hPa (Figure 7), and 850 hPa (Figure 8) from the WRF simulation were matched to the relevant fields in the ERA5 dataset (Figures 2, 3, and

4). This comparative analysis aimed to assess the model's ability to accurately replicate key atmospheric features and ensure consistency with observed patterns at different atmospheric levels. The comparison at the 1000 hPa level revealed that the WRF effectively simulates the temperature gradient and accurately represents the different pressure systems, with only minor discrepancies in the positioning of their centers and the extent of their horizontal coverage. Furthermore, the extended center of the RST over the EM and SA throughout the study period exhibited a high degree of similarity between the WRF simulation and ERA5 data. This agreement is evident by tracing the 100 gpm contour line and observing its spatial extent in the geopotential height field, both east and west of the Red Sea (Figures 2 and 6). The alignment of these features underscores the model's capability to capture the key atmospheric patterns observed during the study.

The 500 hPa charts during the period of the study show that the upper-air trough spatial distribution in the WRF simulation and the ERA5 dataset is very consistent. The alignment of these patterns indicates that the WRF effectively describes the structure and position of the upper-level trough. The only notable difference lies in minor deviations, with variations of up to ±30 gpm observed in the cut-off low center (Figures 3 and 7). These small discrepancies highlight the model's strong performance in accurately reproducing the synoptic-scale features at the 500 hPa level.

Figure 8 presents the horizontal distribution of temperature advection and geopotential height (gpm) at the 850 hPa level, as derived from the WRF simulation. This figure also highlights the baroclinic zone present in the lower atmospheric layer throughout the study period. When comparing Figure 8 with the corresponding ERA5 data shown in Figure 4, it is evident that the horizontal distribution of geopotential height is nearly identical between the two datasets. However, there are minor discrepancies in the geopotential height values, consistent with the small differences observed at the 1000 and 500 hPa levels. These variations do not significantly affect the overall spatial agreement, underscoring the model's capability to replicate key synoptic features at this level. However, the real difference between the two figures lies in the thermal advection. We observe that the horizontal distribution of thermal advection is consistent between the WRF and ERA5 datasets, with similar patterns of heating and cooling. Nevertheless, the model exhibits a tendency to overestimate the intensity of both cold and warm advection when compared to the ERA5 dataset. This overestimation is evident in the stronger temperature gradients and advection patterns simulated by the model, which slightly exaggerate the actual atmospheric dynamics reflected in the ERA5 analysis. Such differences may influence the depiction of thermal and baroclinic processes within the study domain. From a broader perspective, the model effectively captured the spatial patterns of cold and warm advection, as well as the associated baroclinic zones, demonstrating its capability to represent these features reasonably well. However, the model exhibited a tendency to overestimate the intensity of these advection processes when compared to the ERA5 dataset. This discrepancy can be attributed to several factors, including the choice of convective parameterization schemes, spatial resolution, model physics parameterizations, and the quality of boundary and initial conditions. These factors, as highlighted in the precipitation comparison section, have a significant impact on the accuracy of the simulated atmospheric processes. Addressing these challenges and refining the model's configuration to better replicate such scenarios remains an important area for future research, emphasizing the need to carefully evaluate and select appropriate settings to enhance model performance.

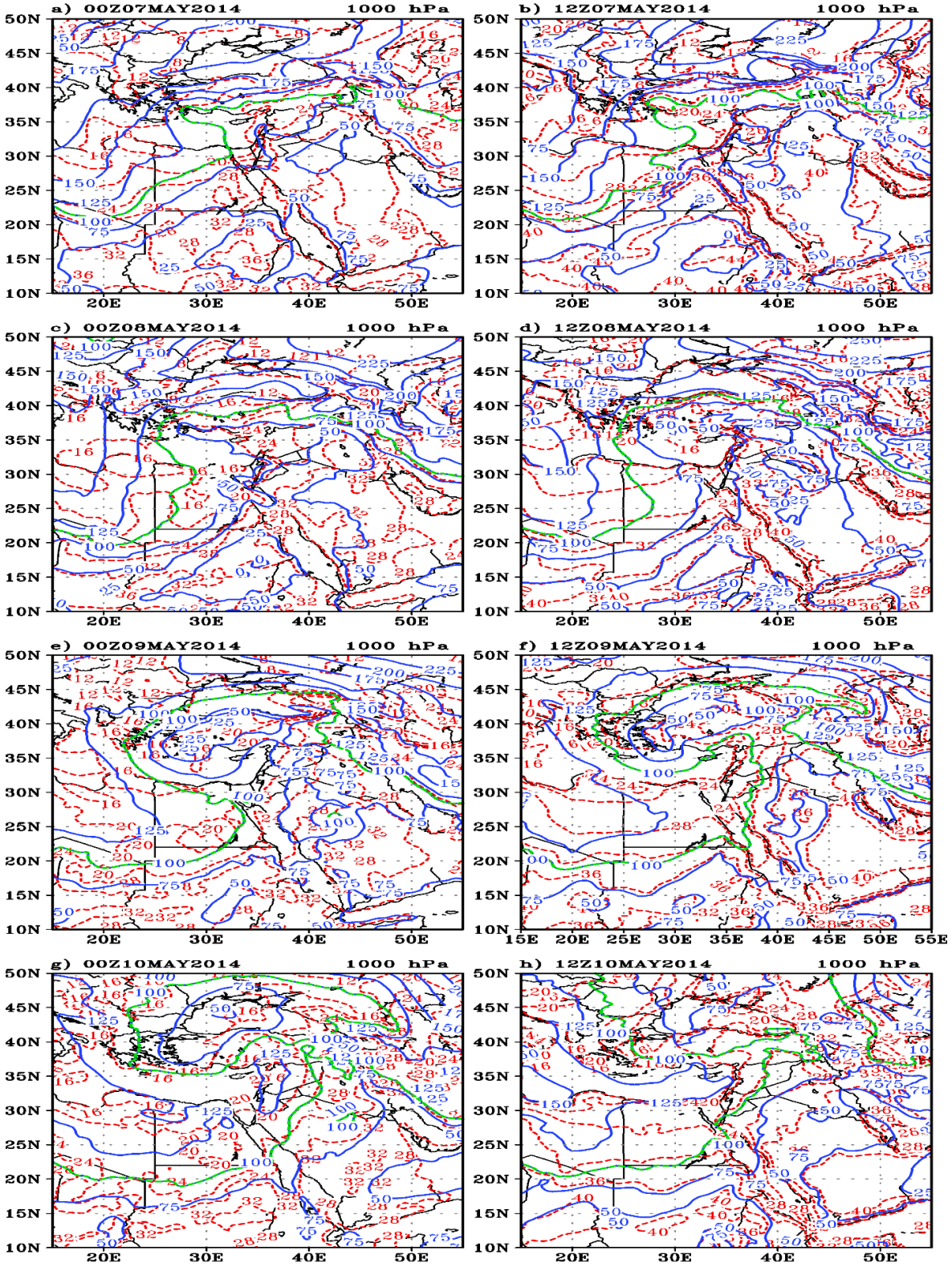

Figure 6. 1000 hPa height contours (blue) and temperature (red) at 00Z and 12Z for 07 to 10 May 2014 from WRF output.

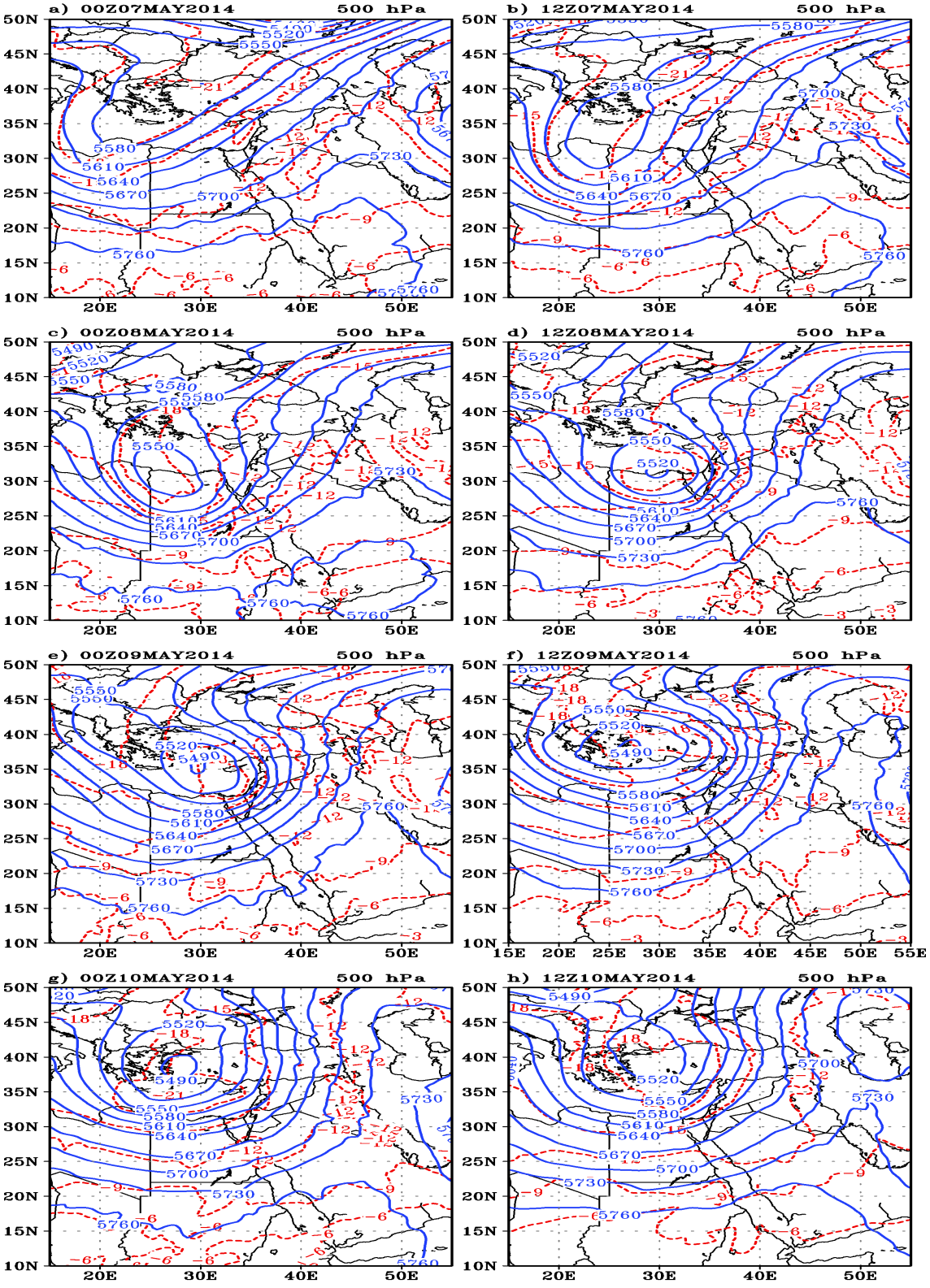

Figure 7. 500 hPa geopotential height (solid blue lines) and temperature (red dotted) at 00Z and 12Z for 07 to 10 May 2014 from WRF output.

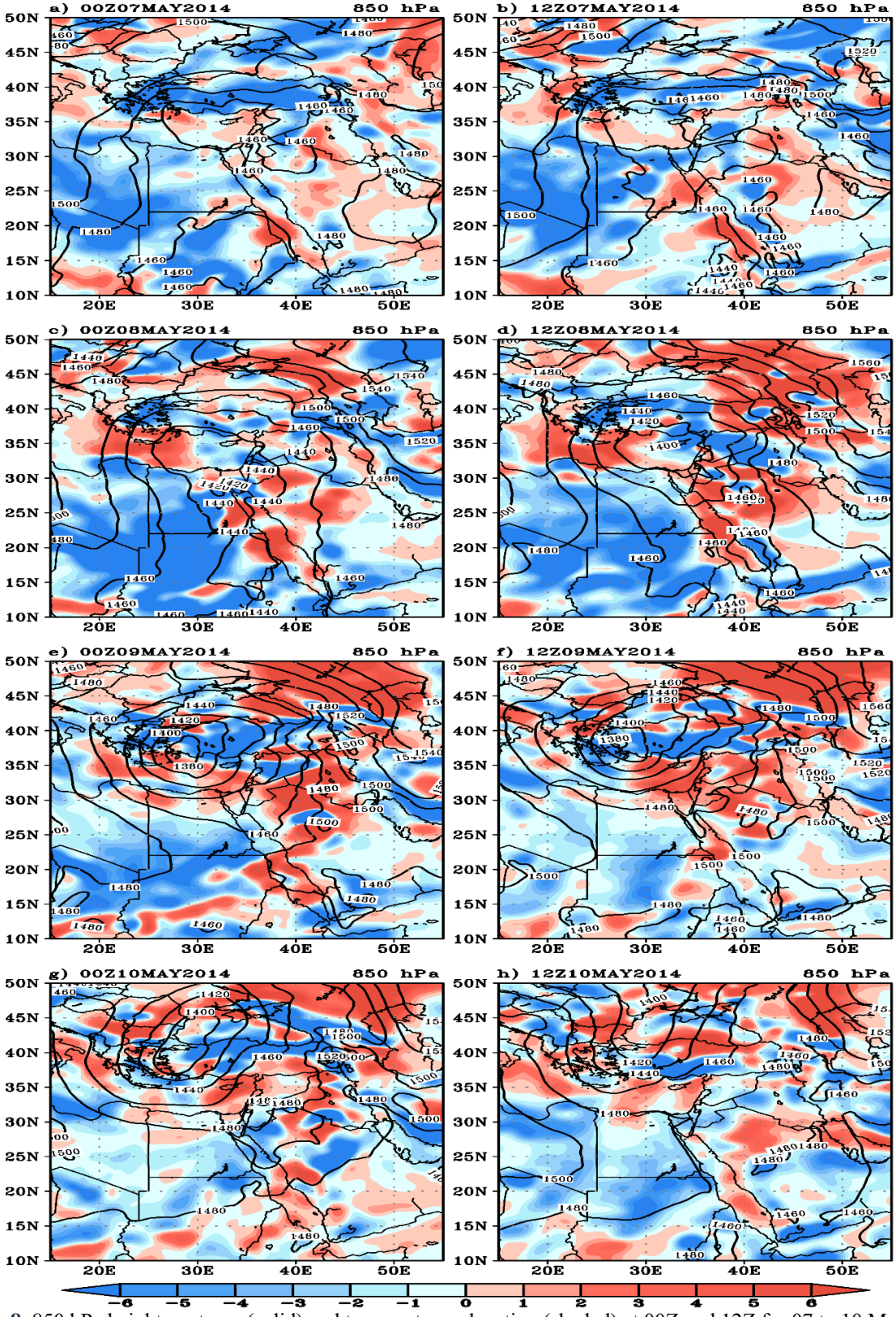

Figure 8. 850 hPa height contours (solid) and temperature advection (shaded) at 00Z and 12Z for 07 to 10 May 2014

3. Conclusion

This study aimed to simulate the horizontal distribution and intensity of a significant rainfall event that occurred over central and western SA from 8 May 2014, using WRF model. The analysis of the synoptic patterns demonstrated that the primary driver of this significant rainfall event was the dynamic interaction between a cold upper air trough, associated with a midlatitude cyclone, and the lower-level RST. The upper-level cold trough provided the necessary atmospheric instability by introducing cold air aloft, while the RST at the lower levels played a pivotal role in transporting warm, moisture-laden air masses from the Red Sea and the Arabian Sea. This moisture advection towards western SA and its surrounding regions created a conducive environment for enhanced convection and precipitation, culminating in the observed rainfall event. The model effectively simulated the spatial distribution patterns of rainfall, demonstrating a notable level of agreement with TRMM data. However, it tended to overestimate the daily accumulated rainfall totals by approximately 10-20%, especially in areas experiencing intense precipitation. These regions included the RS area and the northwestern parts of SA, where the model produced higher rainfall magnitudes compared to satellite observations. Additionally, the synoptic properties and spatial patterns of warm and cold advection (baroclinicity) may be accurately represented by the model. However, the WRF exhibited a tendency to overestimate the intensity of both cold and warm advection processes when compared to the ERA5 reanalysis data. The overestimation of rainfall by the model compared to TRMM data, along with discrepancies in synoptic features and thermal advection patterns, can likely be attributed to limitations in the model's spatial resolution, physical parameterization schemes, and its capability to accurately simulate localized convective processes. These shortcomings highlight areas where the model may not fully capture the complexities of atmospheric dynamics. To enhance the accuracy of rainfall predictions, future research should prioritize refining model resolution, improving physical parameterization techniques, and integrating more extensive observational datasets to better represent mesoscale and convective phenomena.

References

Abdeldym, A.; Basset, H.A.; Sayad, T.; Morsy, M. Kinetic energy budget and moisture flux convergence analysis during interaction between two cyclonic systems: Case study. Dyn. Atmos. Oceans 2019, 86, 73–89.

Aligo, E.A., Ferrier, B. and Carley, J.R., 2018. Modified NAM microphysics for forecasts of deep convective storms. *Monthly Weather Review*, *146*(12), pp.4115-4153.

Al-Khalaf, A.K.; Abdel Basset, H. Diagnostic study of a severe thunderstorm over Jeddah. Atmospheric and Climate Sciences 2013, 3, 150-164.

Almazroui, M. Sensitivity of a regional climate model on the simulation of high intensity rainfall events over the Arabian Peninsula and around Jeddah (Saudi Arabia). Theor. Appl. Clim. 2011, 104, 261–276.

Almazroui, M.; Raju, P.V.S.; Yusef, A.; Hussein, M.A.A.; Omar, M. Simulation of extreme rainfall event of November 2009 over Jeddah, Saudi Arabia: The explicit role of topography and surface heating. Theor. Appl. Clim. 2018, 132, 89–101, doi:10.1007/s00704-017-2080-2.

Al-Mutairi, M., Abdel Basset, H., Morsy, M. and Abdeldym, A., 2019. On the effect of red sea and topography on rainfall over Saudi Arabia: Case study. *Atmosphere*, *10*(11), p.669.

Chawla, I.; Osuri, K.K.; Mujumdar, P.P.; Niyogi, D. Assessment of the Weather Research and Forecasting (WRF) model for simulation of extreme rainfall events in the upper Ganga Basin Hydrol. Earth Syst. Sci. 2018, 22, 1095–1117.

De Vries, A.J.; Tyrlis, E.; Edry, D.; Krichak, S.O.; Steil, B.; Lelieveld, J. Extreme precipitation events in the Middle East: Dynamics of the active Red Sea trough. J. Geophys. Res. Atmos. 2013, 118, 7087–7108, doi:10.1002/jgrd.50569.

Deng, L.; McCabe, M.F.; Stenchikov, G.; Evans, J.P.; Kucera, P.A. Simulation of Flash-Flood-Producing Storm Events in Saudi Arabia Using the Weather Research and Forecasting Model. J. Hydrometeorol. 2015, 16, 615–630, doi:10.1175/JHM-D-14-0126.1.

Dudhia, J. A multi-layer soil temperature model for MM5. In Proceedings of the Sixth PSU/NCAR Mesoscale Model Users' Workshop, Boulder, CO, USA, 22–24 July 1996.

El Kenawy, A.M.; McCabe, M.F.; Stenchikov, G.L.; Raj, J. Multi-decadal classification of synoptic weather types, observed trends and links to rainfall characteristics over Saudi Arabia. Front. Environ. Sci. 2014, 2, 37, doi:10.3389/fenvs.2014.00037.

El-Fandy, M.G. The effect of the Sudan monsoon low on the development of thundery conditions in Egypt, Palestine and Syria. Q. J. R. Meteorol. Soc. 1948, 74, 31–38.

Giorgi F, Mearns LO (1999) Introduction to special section: regional climate modeling revisited. J Geophys Res 104:6335–6352

Giorgi, F., Hostetler, S.W. and Brodeur, C.S., 1994. Analysis of the surface hydrology in a regional climate model. *Quarterly Journal of the Royal Meteorological Society*, *120*(515), pp.161-183.

Haggag, M.; El-Badry, H. Mesoscale numerical study of quasi-stationary convective system over Jeddah in November 2009. Atmos. Clim. Sci. 2013, 3, 73–86.

Hasanean, H.; Almazroui, M. Rainfall: Features and Variations over Saudi Arabia, a Review. Climate 2015, 3, 578–626, doi:10.3390/cli3030578.

Hersbach, H., Bell, B., Berrisford, P., Hirahara, S., Horányi, A., Muñoz-Sabater, J., Nicolas, J., Peubey, C., Radu, R., Schepers, D. and Simmons, A., 2020. The ERA5 global reanalysis. *Quarterly Journal of the Royal Meteorological Society*, *146*(730), pp.1999-2049.

Hong, S.Y.; Noh, Y.; Dudhia, J. A new vertical diffusion package with an explicit treatment of entrainment processes, Mon. Weather. Rev. 2006, 134, 2318–2341, doi:10.1175/MWR3199.1.

Huffman, G.J.; Adler, R.F.; Bolvin, D.T.; Nelkin, E.J. The TRMM multi-satellite precipitation analysis (TMPA). In Satellite Rainfall Applications for Surface Hydrology; Springer: Dordrecht, The Netherlands, 2010; pp. 3–22.

Iacono, M.J.; Delamere, J.S.; Mlawer, E.J.; Shephard, M.W.; Clough, S.A.; Collins, W.D. Radiative forcing by long–lived greenhouse gases: Calculations with the AER radiative transfer models. J. Geophys. Res. 2008, 113, D13103, doi:10.1029/2008JD009944.

Jones RG, Murphy JM, Noguer M (1995) Simulation of climate change over Europe using a nested regional-climate model. Part I: assessment of control climate, including sensitivity to location of boundaries. Q J R Meteorol Soc 121:1413–1450. doi:10.1002/qj.49712152610

Kain, J.S. The Kain-Fritsch convective parameterization: An update. J. Appl. Meteorol. 2004, 43, 170–181, doi:10.1175/1520-0450(2004)043<0170:TKCPAU>2.0.CO;2.

Leung, L.R., Ghan, S.J., Zhao, Z.C., Luo, Y., Wang, W.C. and Wei, H.L., 1999. Intercomparison of regional climate simulations of the 1991 summer monsoon in eastern Asia. *Journal of Geophysical Research: Atmospheres*, *104*(D6), pp.6425-6454.

Maussion, F.; Scherer, D.; Mölg, T.; Collier, E.; Curio, J.; Finkelnburg, R. Precipitation seasonality and variability over the Tibetan Plateau as resolved by the High Asia Reanalysis. J. Clim. 2014, 27, 1910–1927.

Mohan, M.; Sati, A.P. WRF model performance analysis for a suite of simulation design. Atmos. Res. 2016, 169, 280–291.

Monin, A.S.; Obukhov, A.M. Basic laws of turbulent mixing in the surface layer of the atmosphere. Contrib. Geophys. Inst. Acad. Sci. USSR 1954, 151, 163–187. (In Russian)

Nobre P, Antonio DM, Sun L (2001) Dynamical downscaling of seasonal climate prediction over Nordeste Brazil with ECHAM3 and NCEP's regional spectral models at IRI. Bull Am Meteorol Soc 82:2787–2796

Ribó, M.; Llasat, M.C. Study of the impact of cyclogenesis at the Mediterranean Sea. In Proceedings of the 11th EGU Plinius Conference on Mediterranean Storms, Barcelona, Spain, 7–10 September 2009; Volume 11, Plinius-11-88.

Samman, A. E.; Gallus Jr, W. A. (2018). A classification of synoptic patterns inducing heavy precipitation in Saudi Arabia during the period 2000-2014. Atmósfera, 31(1), 47-67.

Seth A, Giorgi F (1998) The effect of domain choice on summer precipitation simulation and sensitivity in a regional climate model. J Climate 11:2698–2712

Shiao CH, Juang HMH (2006) Sensitivity study of the climate simulation over East Asia with the CWB regional spectral model. Terr Atmos Ocean Sci 17:593–612

Sylla MB, Coppola E, Mariotti L, Giorgi F, Ruti PM, Dell'Aquila A, Bi X (2010) Multiyear simulation of the African climate using a regional climate model (RegCM3) with the high resolution ERA-interim reanalysis. Climate Dyn 35:231–247. doi:10.1007/s00382-009-0613-9

Sylla, M.B., Gaye, A.T., Pal, J.S., Jenkins, G.S. and Bi, X.Q., 2009. High-resolution simulations of West African climate using regional climate model (RegCM3) with different lateral boundary conditions. *Theoretical and Applied Climatology*, *98*, pp.293-314.

تقييم أداء نموذج WRF لحالة هطول أمطار شديدة في غرب المملكة العربية السعودية

أحمد السمان[1،2]، عبدالله عبد الدايم[2]، ومصطفى مرسي[2]

1قسم الأرصاد الجوية، كلية العلوم البيئية، جامعة الملك عبد العزيز، جدة، 21589. المملكة العربية السعودية.

2مركز التميز لأبحاث تغير المناخ، جامعة الملك عبد العزيز، جدة 21589، المملكة العربية السعودية

مستخلص. تتناول هذه الدراسة أداء نموذج الطقس والبحث والتنبؤ **(WRF)** في محاكاة حدث جوي شديد تميز بهطول أمطار غزيرة وعواصف رعدية، والذي وقع في غرب المملكة العربية السعودية في 8 مايو 2014. سجلت محطة الأرصاد الجوية في مكة المكرمة حوالي 50 ملم من الأمطار خلال هذا الحدث. تم إعداد نموذج **WRF** باستخدام إعدادات بدقة متوسطة ومجموعة متنوعة من مخططات المعايرة لمحاكاة الحدث. تم مقارنة شدة وتوزيع الأمطار المحاكاة بواسطة النموذج مع تقديرات هطول الأمطار من مهمة قياس الهطول الاستوائي **.(TRMM)** تُبرز النتائج نقاط القوة والضعف في نموذج **WRF** في محاكاة الأحوال الجوية الشديدة في غرب المملكة، مما يوفر رؤى لتحسين التنبؤات المستقبلية.